Histogram interpretation for non-imaging laser system pointing estimations

Susan Chandler and Gordon Lukesh

Nukove Scientific Consulting, Ranchos de Taos, New Mexico, USA

This paper presents details of a special algorithm that provides real-time estimates of ground-to-space laser beam system pointing errors. The intent is to provide feedback for adaptive beam control so that such a system can reduce boresight, a static bias in pointing caused by misalignment or systemic static pointing errors. The algorithm requires only the received full aperture time-series signal and does not require imaging nor costly adaptive optics. Effects such as glints, speckle, and atmospheric scintillation do not corrupt the predictions from the algorithm.

Introduction

A ground-based laser system that projects a narrow beam at a space object is subject to pointing disturbances caused by atmospheric turbulence, vibrations, and static mechanical effects. Knowledge of the magnitude of these disturbances provides diagnostics for an experiment. In a laboratory, an imaging focal plane at the target can easily determine the shot-to-shot pointing errors. When only the received time-series signal at a large telescope (~3.5 m) on the ground is recorded, such estimates were not available until the authors devised a method in 1997,[1] which established that considerable information can be taken from the total received time-series signal from ground—space—ground illumination experiments.

The algorithm developed by the authors and described here uses the χ^2 statistical technique, which is ideal for estimation of goodness-of-fit for small data sets to known probability distributions. The method is to predetermine the theoretical probability distributions for data sets using Monte Carlo simulations for a range of pointing disturbances known as jitter and boresight, which are shot-by-shot pointing errors and offsets due to optical misalignment, respectively. The algorithm then uses these probability distributions to provide real-time simultaneous estimates of multiple parameters of a remote sensing target/atmosphere/laser system by testing the hypothesis that small sets (≥ 25) of measured return photons arise from one of these pre-solved probability distributions.[2]

Only the time-series return photon signal, collected over a large aperture (~2—4 m), need to be recorded. Costly imaging systems and adaptive optics do not need to be employed; the main requirement is that the illuminating beam at the target must have a reasonable pattern (for example, Gaussian) or a beam full-width-at-half-maximum (FWHM) main lobe that is not badly corrupted by the atmosphere. Effects such as glints, speckle, and scintillation have been studied extensively. None of these corrupts the predictions of jitter or boresight.

A scenario for a ground—space—ground laser illumination experiment is that a laser is fired through a ground telescope (transmitter) at an orbiting satellite. The reflected light is collected by a detector (receiver) on the ground. This received intensity is used to compute the pointing errors of the laser transmitter. Many ground—space—ground illumination experiments provide data sets that have been collected over a large portion of the satellite pass, where target characteristics, such as orientation and range, change appreciably. Over a short time however, these variables are nearly constant. Small data sets, collected over a short time, are needed for field estimation of laser system pointing. Figure 1 illustrates the basic concept of a ground—space—ground laser illumination experiment, including the laser transmitter, the output beam and its FWHM, and the beam reflected (dotted line) to the ground-based receiver.

A ground-to-space field experiment with a low earth orbit satellite will have an overall envelope for the received intensity. During the engagement, this envelope is bounded by an R^4 curve, where R is the range, as the intensity at the target and at the receiver changes. In previous work,[3] the range effect was accounted for via a standard radiometry equation in the theoretical probability distributions. Recently, simulations have shown that the assumption that R is constant does not effect the determination of the pointing errors, provided that the experimental data is collected reasonably fast. This allows the experimenters to eliminate the measurement of R. When variations in laser energy and beam quality have a long period relative to the experiment repetition rate, these variations can also be ignored. This also greatly simplifies the estimation of jitter and boresight and allows for near-real-time conclusions and feedback due to the very limited data requirements. Post processing, with a full accounting for range and laser variations, may be performed,

although analysis has shown correlation coefficients between estimates for raw data and fully corrected data exceed 0.95.
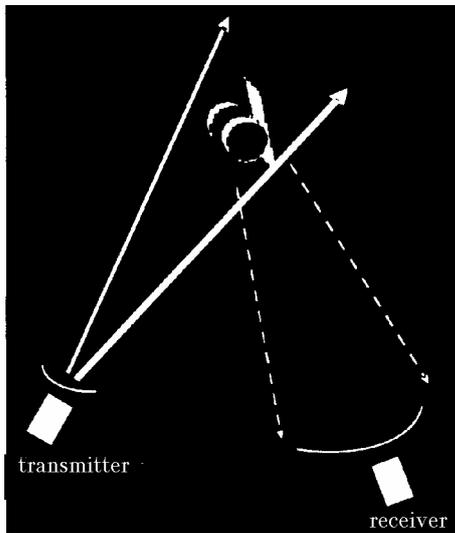
Fig. 1. This figure shows a scenario for a ground–space–ground laser illumination experiment. A laser is fired through a ground telescope (transmitter) at an orbiting satellite. The reflected light is collected by a detector (receiver) on the ground. This received time-series signal is used to compute the pointing errors of the laser transmitter. A typical range to a satellite is 10^6 m and the transmitter and receiver separation is 100 m.

1. Pointing disturbances

In the absence of pointing disturbances, the expected total photon returns will be constant (when corrected for range, laser energy variations, and target orientation changes). Telescope mechanical vibrations and the atmosphere introduce uncontrolled residual errors, even with a tracking system, that cause the laser to miss the target partially or completely. Two measures of disturbances, known as jitter and boresight, are described here. For more details, see previous papers.[1,3]

Jitter is the term for shot-to-shot pointing errors arising from mechanical vibrations and residual tracking errors. It is modeled as a two-axis (x, y) uncorrelated error subject to Eq. (1), where σ_j is the single axis 1–σ specification and x and y are angular units. During an experiment, it is assumed that the jitter is drawn from this distribution. On a shot-to-shot basis, random draws were taken for the x-axis and the y-axis independently. The goal is to determine σ_j from only the received total time-series intensities:

$$J(x,y) = \frac{1}{2\pi\sigma_j^2}\exp\left(\frac{-(x^2 + y^2)}{2\sigma_j^2}\right). \qquad (1)$$

Boresight is a fixed residual optical misalignment, or bias, during a specific engagement. Boresight errors may arise from incorrect commands to a beam steering mirror or an optical misalignment. Boresight

may also arise from the simple geometry of an engagement: when a satellite is tracked while it is sunlit, but with the ground site in darkness (known as terminator mode), tracking using solar illumination will introduce an offset of about one-half the size of the object.

To simulate an engagement with jitter and boresight, it is a simple matter to replace, in Eq. (1), x with $x - x_b$ and y with $y - y_b$ where (x_b, y_b) is the boresight offset vector. This results in random draws of beam position that are centered on (x_b, y_b). The beam was offset by a random draw and the integrated intensity at target was recorded on a shot-by-shot basis. In the absence of downlink variations, the intensity is proportional to the received signal and thus ideal for estimation by the pointing algorithm.

2. The histogram approach using predetermined probability distributions

The familiar χ^2 test is used to compare small data sets with predetermined probability distributions. There are two fundamental equations used for analysis. The first is the equation for χ^2:

$$\chi^2 = \sum_i \frac{(N_i - n_i)^2}{n_i}, \qquad (2)$$

where the N_i are the measured frequencies and the n_i are the expected frequencies. For a typical use of the algorithm, $i = 5$ bins and intensities from 25 shots are used. The expected frequencies (n_i) for data arising from the same distribution as the parent distribution are [5 5 5 5 5].
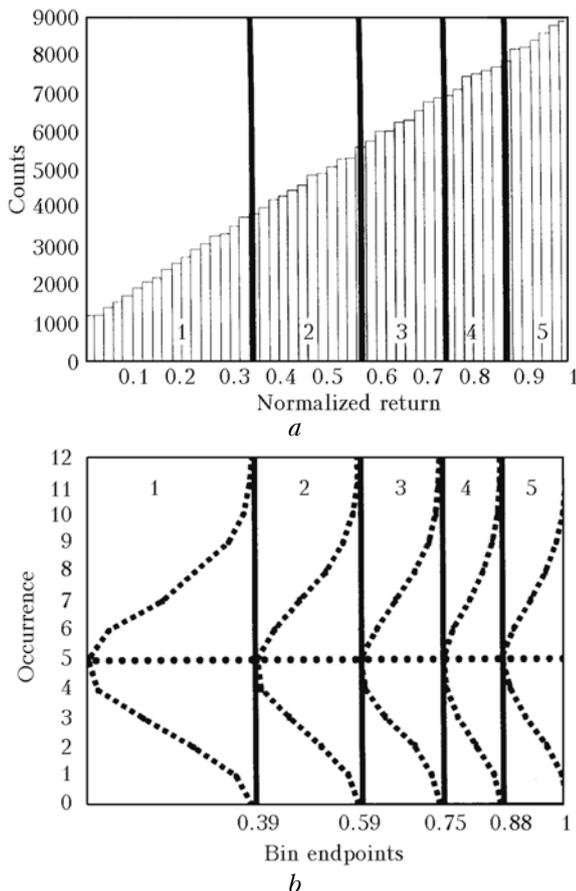
The second equation, closely associated with χ^2, is the statistical confidence Q. The formal equation for Q involves the incomplete gamma function and is shown in Eq. (3):

$$Q(\chi^2 \mid \nu) = gammq\left(\frac{\nu}{2},\frac{\chi^2}{2}\right). \qquad (3)$$

Here ν is the number of degrees of freedom; for the $i = 5$ case, $\nu = 4$. A set of 25 measured intensities that results in all $N_j = 5$ will yield $\chi^2 = 0$ and $Q = 1$. One would not reject the hypothesis that the data arose from the predetermined distribution. It is considered a perfect match.

Fundamental to the application of the algorithm is that the data must follow reasonable statistics.[4] This is to be interpreted as follows: when Monte Carlo simulations are performed for a specific hypothesis and tested as to whether the data arose from the same hypothesis, the occurrences per bin should follow Gaussian, Poisson or, more generally, binomial statistics. Consider, for example, the case of tosses of a fair coin: the expected frequency of heads is five, but the distribution about the mean is Gaussian.

Figure 2 shows an example. The data in Fig. 2a shows the probability distribution for 10^5 simulated shots under the hypothesis that jitter is $0.28 \times$ FWHM, and boresight is $0.56 \times$ FWHM. Figure 2a also shows the equal count bins that are the foundation of the algorithm. A value of zero on the x-axis of the histogram in Fig. 2a represents a total failure of the laser to illuminate the target, while a value of unity represents a perfect illumination of the target. The hypothesis presented represents excellent pointing and often occurred during recent US Air Force experiments. Figure 2b shows the result of 10^4 simulations of 25 shots having the same hypotheses as Fig. 2a. The expected frequency per bin is five and the distributions within each bin peak at five and follow binomial statistics, that is the mean $\mu = np = 5$ and the variance $\sigma^2 = np(1 - p) = 4$. (Here, $p = 0.2$ is the probability of falling into one bin, and $n = 25$ is the number of points.)

The algorithm provides estimates of pointing errors throughout a satellite pass using streaming data, that is, shots 1–25, 2–26, 3–27, etc. Pointing estimates are available after the first 25 shots. These nearly immediately available estimates show the true strength of the χ^2-based algorithm. A running average is also provided, using 200 successive 25-point estimates to smooth the estimates. The pointing estimates from the algorithm, both for simulated data and laboratory experiments, have proven exceptional.

3. Field data

The InfraRed Astronomical Satellite (IRAS) was successfully illuminated during several experiments performed by the United States Air Force Research Laboratory at the Starfire Optical Range on Kirtland Air Force Base in New Mexico. The intensity of the photons measured during one pass by the receiver is shown in Fig. 3. The measured range to IRAS is also shown by the solid line. The R^4 effect in the data is clearly visible. (The non-smooth nature of the range is due to the fact that the data is presented by shot number and the laser did not fire at a uniform repetition rate.) The tremendous variation in the signal from pointing errors is apparent. The beam FWHM is approximately 3.5 μrad, typical of a recent experiment, and a wave optics analysis established that the central lobe is nearly Gaussian.
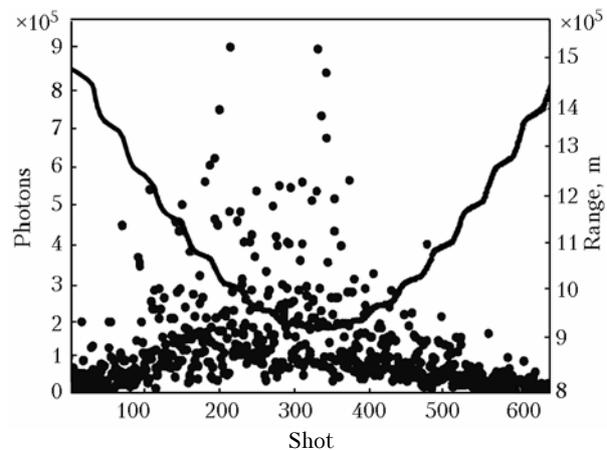

a

b

Fig. 2. This figure shows one example of the underlying statistics of the histogram-matching algorithm. Figure *a* is a histogram of 10^5 simulated return intensities from a case with excellent pointing. The data is divided equally among 5 bins for use in χ^2 testing. Unity on the x-axis represents perfect pointing and zero represents a complete miss. Figure *b* shows the corresponding distribution within each bin obtained from 10^4 realizations of 25 shots. Each is a binomial distribution and peaks at the expected 5 occurrences per bin.


Fig. 3. This shows the photons measured from an IRAS engagement (black dots) performed during a recent experiment in New Mexico, USA. The range (R) to the satellite is shown by the solid line and is not smooth since the data was recorded by shot number instead of time. More photons are measured as the satellite comes closer to the observer due to the R^4 effect.

For the Monte Carlo simulations used to pre-determine probability distributions, the far-field beam pattern is either taken to be diffraction limited or computed from wave propagation through the atmosphere. Figure 4 shows a slice of a far-field beam with wavelength of 1 μm projected from a 0.25 m diameter telescope. The telescope is at an altitude of 3×10^3 m, typical of a mountaintop observatory. The beam propagates through the atmosphere to 3×10^4 m,

then through vacuum to the satellite at 10^6 m. The atmosphere is modeled with 10 phase screens. The far-field pattern has minimum degradation when compared to a purely vacuum propagation. This is typical of a high-altitude transmitter with a small (0.25 m) aperture. In this case, no transmitter adaptive optics was used.
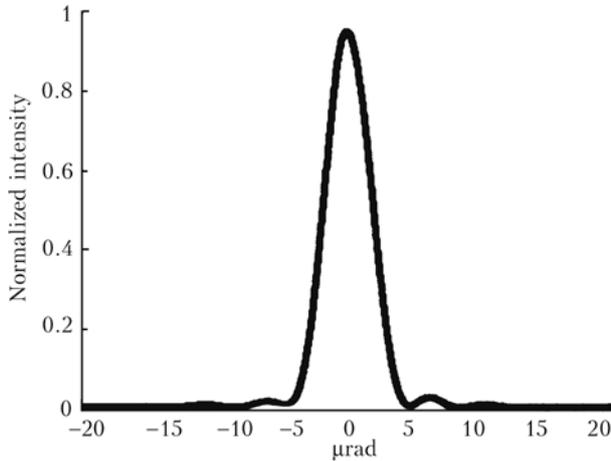

Fig. 4. This graph is a cross section through the (normalized) peak intensity of a far-field beam numerically propagated from a 3×10^3 m ground site to 10^6 m. The simulation wavelength was 1.0 μm and the aperture was 0.25 m. Ten atmospheric phase screens were used. There is minimum corruption when compared to a vacuum-propagated, diffraction-limited beam.
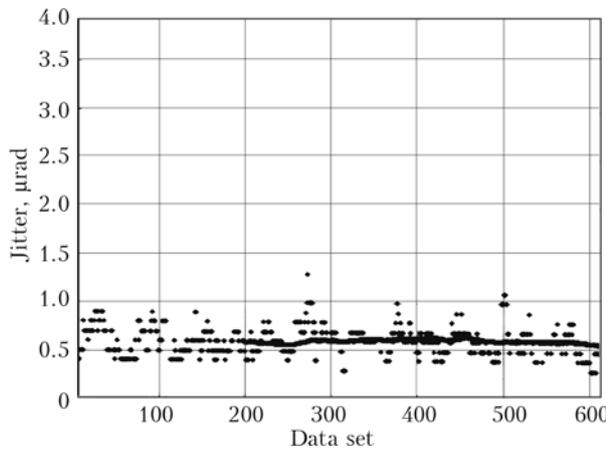
Fig. 5. This figure shows the jitter estimate for the IRAS engagement in Fig. 3. Each black dot shows the jitter estimate from a data set. Each data set is from 25 measured intensities. The 200-point running average is indicated by the solid line. The jitter estimate of approximately 0.6 μrad indicates very good atmospheric seeing and excellent tracker performance during the satellite pass.

The jitter estimates obtained for this pass are shown in Fig. 5. Successive data sets of measured photon intensity from 25 shots (1–25, 2–26, 3–27...) were used for each jitter estimate and are shown as the black dots in Fig. 5 and for each boresight estimate in Fig. 6. The jitter estimates varied from 0.4 μrad to 1.3 μrad, with a 200-point moving average of 0.6 μrad, or 0.17 × FWHM. This jitter is

indicative of the excellent atmospheric seeing and exceptional tracker performance that approaches the anisoplanatic limit. The boresight estimate was approximately 2.5 μrad, or 0.71 × FWHM.
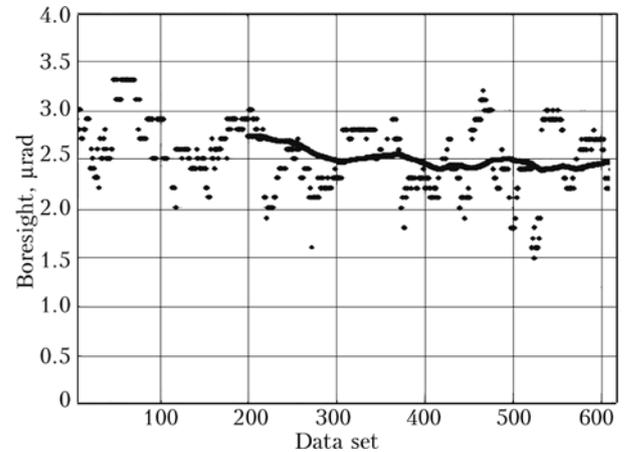
Fig. 6. This plot shows the boresight estimate (black dots) for each data set (from 25 measured intensities) for the IRAS data shown in Fig. 3. The 200-point running average (solid line) indicates a large pointing offset of ~2.5 μrad. This was determined to be due to the engagement geometry and passive tracking with the transmitter–satellite–sun angle at approximately 90°.

The ground-to-space satellite experiment operated in terminator mode, where the transmitter/receiver site was in the dark, but the satellite was sunlit, shortly after sunset or shortly before sunrise. Using solar illumination, the tracker pointed at the brightest region of the satellite, which is also referred to as the solar illumination center-of-mass (COM). Since the earth site-to-satellite-to-sun angle is approximately 90°, only one side of the satellite is illuminated. Thus, the solar COM is offset from the satellite physical center by half its size. This introduces an immediate pointing bias, shown in Fig. 6. A correction for this bias is shown in Fig. 7.
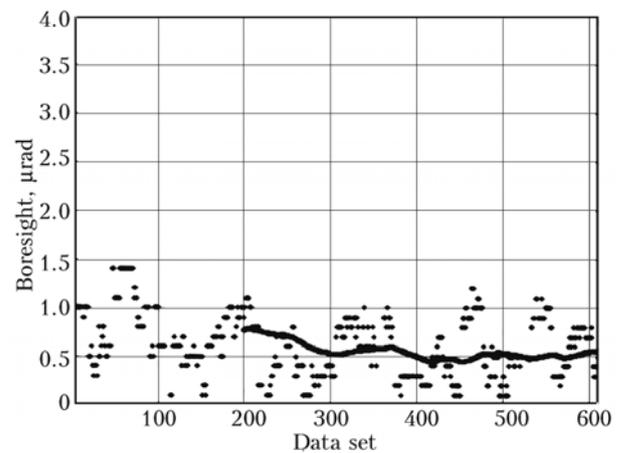
Fig. 7. This plot shows each data set (25 point) boresight estimate (black dots) for the IRAS data shown in Fig. 3, but with a 2 μrad solar offset included in the model. The 200-point running average (solid line) indicates a small pointing offset of ~0.5 μrad.

When a 2 μrad offset was included in the model, a 0.5 μrad pointing boresight resulted.

4. Noise sources

Experiments that transmit a laser to a remote object encounter three types of noise in addition to pointing errors. These are referred to as speckle, atmospheric scintillation, and glints. Speckle arises from the self-interference of a coherent laser light as it propagates from an optically rough (Lambertian) target to the ground receiver. Atmospheric scintillation occurs due to refraction of the reflected beam as it passes through the atmosphere. Different path lengths cause constructive and destructive interference. Numerous experts have studied the theory of speckle and scintillation.[5] Glints are transient effects caused by the chance alignment among the transmitted beam, a flat surface or retro-reflector on the target, and the receiver. The three noise sources have been shown to have no deleterious affect on pointing estimation.

4.1. Speckle

Speckle arises when a coherent laser reflects off an optically rough surface, that is, a surface with a peak-to-valley deviation of about one wavelength. Such surfaces are referred to as Lambertian. Nominal speckle size is $R\lambda/D_{targ}$, where R is the range, λ is the laser wavelength, and D_{targ} is the target dimension. For example, when illuminated by a visible laser a target with dimension 2 m at a range of 10^6 m will produce speckles on the ground of about 0.22 m. The issue is to determine how a speckle pattern affects the received intensity in the presence of pointing errors.

To simulate a speckle pattern numerically, a square target of 128×128 pixels on a 2048×2048 grid was created with a uniform intensity and random pixel-by-pixel phase. A random phase was drawn for each simulated shot, providing a random complex field across the object on a shot-by-shot basis. This emulates the motion of the object relative to the receiver. Propagation to the receiver was performed using standard Fourier optical analysis. On a shot-to-shot basis, the receiver measured the total intensity of each speckle pattern under the assumption of perfect beam pointing. The total aperture time-series data was then normalized by the intensity from a perfectly pointed shot. This provides a probability distribution that represents the speckle noise integrated by the aperture. For simulated data with specified pointing errors, the aperture integration noise is applied to the simulated returns. The resulting data is processed to provide pointing estimates. Speckle can corrupt focal plane data. The fact that the pointing algorithm does not require a focal plane allows for aperture averaging of the speckle on a shot-by-shot basis. For the example above, there are 16 speckles (linearly) across the aperture. The aperture averaging results in a

Gaussian distribution about unity with a $1 - \sigma$ standard deviation less than 0.03. Including this noise in simulated data results in estimates of jitter and boresight that are virtually identical to estimates without speckle noise.

While imaging systems, whether focal- or pupil-plane, will be corrupted by speckle, the algorithm developed by the authors is not affected. The example discussed was for 16 speckles (linearly) across the aperture but with a few as two speckles across the aperture, good pointing estimates may be obtained, although with a definable and repeatable bias. Such a bias is not an impediment to pointing estimation as it may be accounted for in software.

4.2. Atmospheric scintillation

A second noise source is known as scintillation. This occurs due to the interference of multiple paths through atmospheric refraction as the beam propagates to the ground. Scintillation patterns were obtained using a commercially available wave propagation code. For this analysis, a uniform beam was propagated from 3×10^4 m to a receiver at an altitude of 3×10^3 m. Ten phase screens were used to emulate a typical high mountain observatory. One thousand shots were simulated for the analysis, each with a new randomly chosen set of phase screens to ensure independent results. Total intensity was calculated across a 3.5 m aperture. The values were normalized to the mean of the 10^3 realizations. The total variation, less than 2%, was found to be less than that from speckle noise and has no effect on pointing estimation.

4.3. Glints

Glints are the brighter than expected returns caused by the chance alignment of a flat surface or natural retro-reflector with the transmitter and receiver. Flat surfaces can give rise to returns approximately an order of magnitude greater than expected and retro-reflectors can produce returns several orders of magnitude higher than expected. Glints are by nature transient, often occurring for only one illumination as the target rotates relative to the ground site. Many glints were observed during recent field experiments. Because the algorithm uses 25 and 200 points for estimates, neither type of glint has any impact on pointing estimation.

Conclusions

This paper has described a software algorithm, under development by the authors, which has the capability to provide real-time estimates of laser system pointing performance such as jitter and boresight, and to provide feedback for adaptive control of experiments. The algorithm has been repeatedly verified via simulations and in the laboratory, and has been used in prototype-form for field analysis. The algorithm is resilient to speckle, scintillation, and the effects of glints because it uses

25-point data set of the full aperture integrated time-series. It does not require a complicated imaging or adaptive optics system. Forthcoming efforts include developing the algorithm as a commercial package, with links to external experiments.

Acknowledgments

References

1. G. Lukesh, S. Chandler, and D.G. Voelz, Appl. Opt. **39**, 1359—1371 (2000).
2. P.E. Greenwood and M.S. Mikulin, *A Guide to Chi-Squared Testing* (John Wiley & Sons, New York, USA, 1996).
3. S. Chandler, G. Lukesh, D. Voelz, S. Basu, and J.A. Sjogren, Proc. SPIE **5572**, 163—174 (2004).
4. W.H. Press, S.A. Teukolsky, W.T. Vetterling, and B.P. Flannery, *Numerical Recipes in FORTRAN: The Art of Scientific Computing,* 2nd ed. (Cambridge University Press, Cambridge, UK. 1992).
5. J.C. Dainty, ed., *Laser Speckle and Related Phenomena* (Springer-Verlag, Heidelberg, Germany, 1984).